Applied Energy 307 (2022) 118244

Contents lists available at ScienceDirect

Applied Energy

journal homepage: www.elsevier.com/locate/apenergy

Fast charging design for Lithium-ion batteries via Bayesian optimization

Benben Jiang [a], Marc D. Berliner [b], Kun Lai [a], Patrick A. Asinger [b], Hongbo Zhao [b], Patrick K. Herring [c], Martin Z. Bazant [b], Richard D. Braatz [b,*]

[a] Department of Automation, Tsinghua University, Beijing, China
[b] Department of Chemical Engineering, Massachusetts Institute of Technology, Cambridge, MA, USA
[c] Toyota Research Institute, Los Altos, CA, USA

HIGHLIGHTS

- A machine learning strategy is proposed for optimizing rapid charging protocols.
- The strategy explicitly includes constraints that limit battery degradation.
- The approach converges more quickly than other published optimization strategies.
- The performance is quantified for varying number of current steps in the protocol.
- Three CC-step protocol charged 126.6 s and 14.0 s faster than the one and two CC-step protocols.

GRAPHICAL ABSTRACT

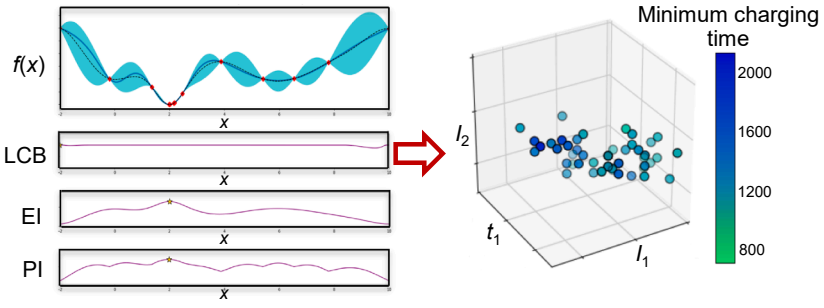

ARTICLE INFO

Keywords:
Fast charging optimization
Data-driven optimization
Bayesian optimization
Gaussian process regression
Acquisition function
Lithium-ion batteries

ABSTRACT

Lithium-ion batteries are one of the most commonly used energy storage device for electric vehicles. As battery chemistries continue to advance, an important question concerns how to efficiently determine charging protocols that best balance the desire for fast charging while limiting battery degradation mechanisms which shorten battery lifetime. Challenges in this optimization are the high dimensionality of the space of possible charging protocols, significant variability between batteries, and limited quantitative information on battery degradation mechanisms. Current approaches to addressing these challenges are model-based optimization and grid search. Optimization based on electrochemical models is limited by uncertainty in the underlying battery degradation mechanisms and grid search methods are expensive in terms of time, testing equipment, and cells. This article proposes a fast-charging Bayesian optimization strategy that explicitly includes constraints that limit degradation. The proposed BO-based charging approaches are sample-efficient and do not require first-principles models. Three different types of acquisition function (i.e., expected improvement, probability of improvement, and lower confidence bound) are evaluated. Their efficacies are compared for exploring and exploiting the parameter space of charging protocols for minimizing the charging time for lithium-ion batteries described by porous electrode theory. The probability-of-improvement acquisition function has lower mean and best minimum charging times than the lower-confidence-bound and expected-improvement acquisition functions. We quantify the decrease in the minimum charging time and increase in its uncertainty with increasing number of current steps used in charging protocols. Understanding ways to increase the convergence rate of Bayesian optimization, and how the convergence scales with the number of degrees of freedom in the optimization, serves as a baseline for extensions of the optimization to include battery design parameters.

* Corresponding author.
E-mail address: braatz@mit.edu (R.D. Braatz).

https://doi.org/10.1016/j.apenergy.2021.118244
Received 27 July 2021; Received in revised form 6 November 2021; Accepted 19 November 2021
Available online 30 November 2021

1. Introduction

Lithium-ion batteries are ubiquitous in a wide range of applications including cellphones, laptops, automotive vehicles, and smart grids, due to high energy and power densities [1,2]. As battery chemistries continue to advance, an important question concerns how to determine charging protocols that best balance the desire for fast charging while limiting battery degradation mechanisms which shorten battery lifetime [3,4]. The operating temperature during battery charging is also of importance, as battery degradation is a strong function of the temperature, and high currents can result in excessive heat generation leading to the possibility of thermal runaway [5].

Challenges in the optimization of charging strategies are the high dimensionality of the space of possible charging protocols, significant variability between batteries, and limited quantitative information on battery degradation mechanisms. Grid search [4,6] and model-based optimization [7,8] are two approaches for probing the large battery operating parameter space. Grid search, which experimentally tests protocols from across the parameter space, including repeats to quantify variability, is accurate but expensive in terms of time, testing equipment, and cells. The use of battery models to optimize operating conditions *in silico* has been proposed as a way to reduce experimentation time. Yin and Choe [9] proposed a nonlinear model predictive control (NMPC) strategy for optimizing the charging current at different states of charge while limiting lithium plating and side reactions. Zhang *et al.* [10] developed an enhanced thermal model-based charging method to balance charging time and temperature rise, while satisfying polarization constraints. Yin *et al.* [11] presented and experimentally validated an alternative NMPC strategy that accounts for the reaction rates of solid electrolyte interphase (SEI) formation and lithium plating. Xu *et al.* [12] proposed a multi-stage charging strategy for lithium-ion batteries to minimize capacity fade accounting for the increase of SEI layer, in which an electrochemical-thermal-capacity fade coupled model is used to estimate battery internal states, followed by using dynamic programming optimization to obtain charging current profiles. Li *et al.* [13] proposed a health-aware charging method that combines an ensemble transform Kalman filter for state estimation with a Proportional-Integral controller that is triggered by physical constraints. Romagnoli *et al.* [14] proposed a computationally efficient reference governor method for fast charging while ensuring safety constraints. However, optimization based on electrochemical models faces two key challenges: (i) Existing battery models do not describe all of the details of the degradation mechanisms and the effects of manufacturing variations [15,16]. The performance of model-based approaches is therefore limited by uncertainty in the underlying battery degradation mechanisms – especially in the early stage of development when a new battery chemistry is being introduced to the market. (ii) The electrochemical models that describe the details of degradation mechanisms in Li-ion batteries are described by hundreds or even thousands of states, which results in an expensive large-scale optimization problem when used to compute charging protocols [16,17]. The issues mentioned above can be addressed by applying a model-free Bayesian optimization (BO) framework for fast charging design.

Bayesian optimization (BO) is a machine learning approach for the global optimization of objective functions that are expensive to evaluate and possibly noisy [18,19], which are the characteristics of the objective function in the fast-charging optimization problem for lithium-ion batteries. A BO approach comprises a surrogate model and an acquisition function. A surrogate model is an inexpensive probabilistic model such as a Gaussian process used for approximating the expensive objective function [18]. The role of the acquisition function, on the other hand, is to define a sample-efficient probing of the space of parameters by balancing exploration and exploitation [19,20].

BO approaches have been proposed for a variety of applications including robot path planning [21], autonomous driving policy determination [22], network sensor placement [23], and hyperparameter tuning for complex machine learning algorithms (e.g., deep convolutional neural network) [24]. Investigations into the application of BO to fast-charging design, however, are limited. In one study [6], a BO algorithm was used to optimize fast-charging protocols by formulating the charging problem as the maximization of the battery cycle life in a fixed charging time. Although it is well established that the performance of a BO algorithm on its acquisition function,[1] Ref. [6] considered only one such function: the upper confidence bound (UCB).

This article extends the data-driven BO methodology in [6] in several specific ways. First, we minimize the charging time instead of keeping it fixed. Second, we optimize over the choice of acquisition functions (i.e., expected improvement (EI), probability of improvement (PI), and lower confidence bound (LCB) [2]), to determine which has the fastest convergence to an optimal charging protocol. Third, we explicitly include constraints in the fast-charging optimization problem to prevent operating under conditions that are known to induce high degradation rates. It is widely acknowledged that cells degrade faster at elevated temperatures (e.g., >40 °C) or higher voltages (e.g., >4.1 V) [25,26], depending on the battery chemistry (e.g., graphite/lithium iron phosphate). Such bounds approximately maintain the thermodynamic conditions required to avoid irreversible side reactions that could lead to accelerated degradation by consuming lithium inventory or building internal resistance. For example, lithium metal plating on the graphite anode (rather than lithium-ion intercalation) is an important mechanism for reduced battery lifetime when the voltage bound is exceeded during fast charging [27,28], which can also trigger thermal runaway [29]. The nucleation of lithium metal is strongly coupled to heterogeneous "mosaic" phase transformations of lithiated graphite [30], which would require a multiphase porous electrode theory [16] to describe in detail [31], but simply imposing voltage and temperature bounds within traditional single-phase porous electrode theory [32] provides a useful proxy for Li-plating-based degradation in the design of fast charging protocols. As proof of principle, therefore, we impose typical constraints on the maximum temperature (40 °C) and voltage (4.1 V) to determine the optimal fast charging protocol for a standard porous electrode model. We implement the constraints in a manner that does not increase the number of degrees of freedom in the BO, and hence does not increase the number of experiments that would be need to determine a fast-charging protocol. The proposed BO-based charging techniques are evaluated for a simulated graphite/$LiCoO_2$ (LCO) cell, with the parameter values fix to experimental data [32].

The main contributions of this work are

(i) A data-driven BO framework is proposed to optimize fast charging while satisfying constraints that limit battery degradation. The BO-based charging approaches are sample-efficient and do not require first-principles models, in contrast to model-based optimization methods that require detailed quantitative understanding of the underlying battery degradation mechanisms, and grid search methods that test protocols from across the parameter space, which are expensive in terms of testing cells (i.e., sample-inefficient).

(ii) The performance of various acquisition functions (i.e., expected improvement, probability of improvement, and lower confidence bound) is thoroughly compared and discussed for the minimum charging time problem with application to a simulated graphite/$LiCoO_2$ battery. This study analyzes the convergence rate of Bayesian optimization, and how the convergence scales with the number of degrees of freedom in the optimization.

The rest of this article is organized as follows. The BO approach is briefly described in Section 2. The proposed BO approach for battery

[1] The acquisition function is defined in the Methods section.

[2] Ref. [6] used the upper confidence bound (UCB) for solving the optimization formulated as a maximization. This acquisition function is equivalent to the LCB in this article, which formulated as a minimization.

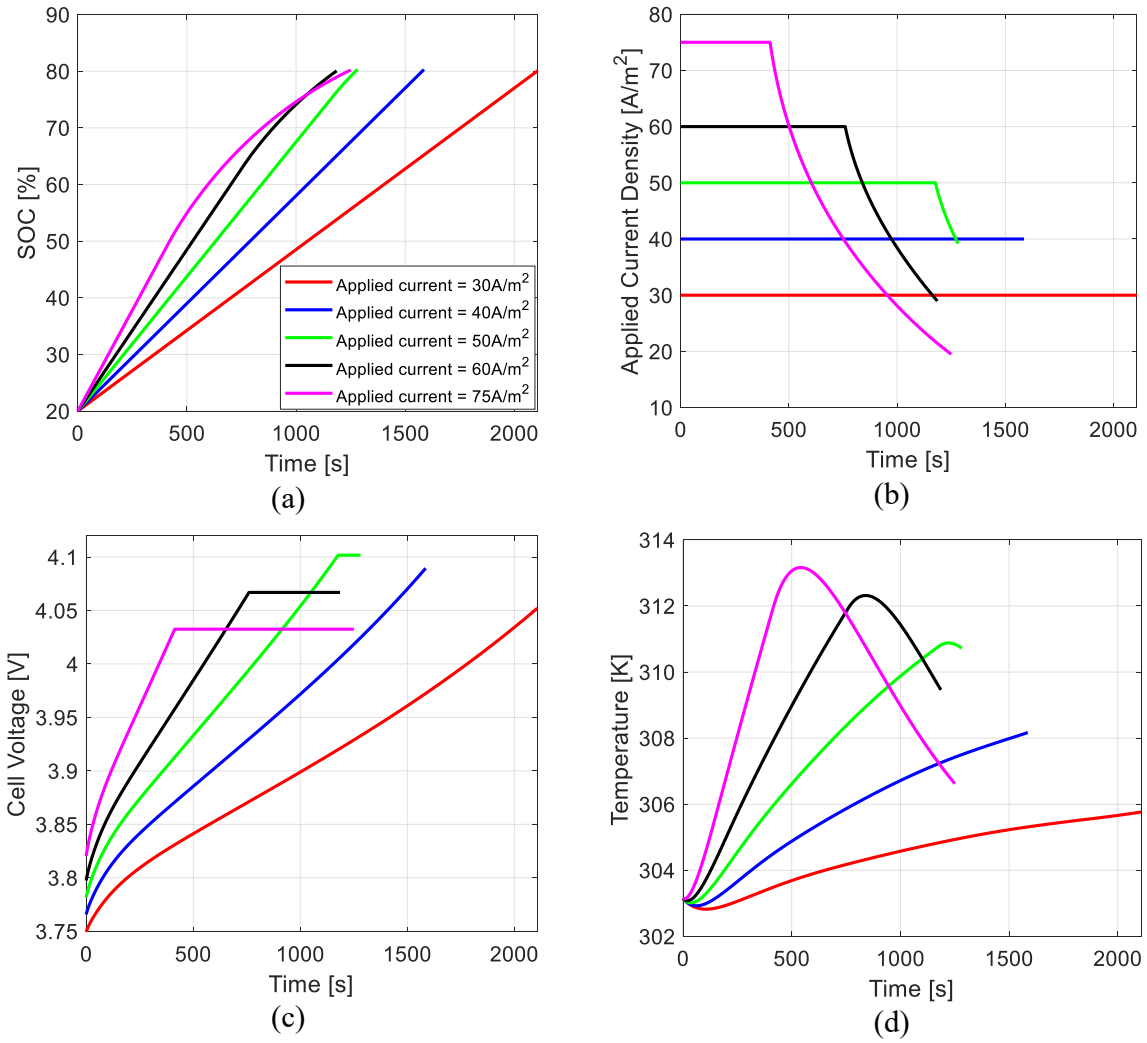

Fig. 1. Charging profiles for one-step charging protocols using the applied currents at 30, 40, 50, 60 and 75 A/m^2: (a) SOC, (b) applied current density, (c) cell terminal voltage, and (d) cell temperature.

optimal charging design is developed in Section 3. The effectiveness of the proposed fast-charging scheme is demonstrated for a simulated graphite/$LiCoO_2$ (LCO) cell in Section 4, followed by conclusions in Section 5.

2. Bayesian optimization approach revisited

The objective of the Bayesian optimization in this article is to minimize a function $f: \boldsymbol{X} \to \mathbb{R}$, where $\boldsymbol{X} \subset \mathbb{R}^d$. At time step t, we select a point $\boldsymbol{x}_t$ and observe a noisy function evaluation

$$y_t = f(\boldsymbol{x}_t) + \varepsilon_t \tag{1}$$

where ε_t is measurement noise following $\varepsilon_t \sim N(0, \sigma^2)$. Let $\boldsymbol{x}^* = \text{argmin}_{\boldsymbol{x}_t \in \boldsymbol{X}} f(\boldsymbol{x}_t)$, and $\Delta_t(\boldsymbol{x}) = f(\boldsymbol{x}_t) - f(\boldsymbol{x}^*)$ measuring the deviation from the optimal function value.

Gaussian process regression is used to build a probabilistic surrogate model of the function f, and then acquisition functions are constructed based on the surrogate model to decide where to sample next. The main features of the probabilistic surrogate model (Gaussian process regression) and acquisition functions (EI, PI, and LCB) are described below.

2.1. Gaussian process regression

Gaussian processes (GPs) are distributions over functions, such that any finite set of function values follows a joint Gaussian distribution [33]. In GP, the mean of $f(\boldsymbol{x})$ is often assumed zero due to lack of *a priori* knowledge, and its covariance for any two inputs $\boldsymbol{x}_i$ and $\boldsymbol{x}_j$ is provided by a kernel function $\kappa(\boldsymbol{x}_i, \boldsymbol{x}_j)$ [33]. Given a set of inputs $\boldsymbol{x} = \{\boldsymbol{x}_i\}_{i=1}^N$ and the corresponding function values $\boldsymbol{f} = \{f(\boldsymbol{x}_i)\}_{i=1}^N$ and measurements $\boldsymbol{y} = \{\boldsymbol{y}_i\}_{i=1}^N$, it can be derived from Eq. (1) that

$$\boldsymbol{y} \tilde{\text{N}}\left(0,\ K_{f,f} + \sigma^2 \boldsymbol{I}_N\right) \tag{2}$$

where $K_{f,f}$ is the N-by-N matrix defined by $[K_{f,f}]_{i,j} = \kappa(\boldsymbol{x}_i, \boldsymbol{x}_j)$. The choice of the kernel function $\kappa(\boldsymbol{x}_i, \boldsymbol{x}_j)$ depends on *a priori* knowledge and data. A commonly used Gaussian kernel is used here [33].

For a new input $\boldsymbol{x}_*$, its GP model output is denoted as f_*. Since the joint distribution of f_* and the observed measurements $\boldsymbol{y}$ follow

$$\boldsymbol{y}, f_* \tilde{\text{N}}\left(0,\ \begin{bmatrix} K_{f,f} + \sigma^2 \boldsymbol{I}_N & K_{f,*} \\ K_{*,f} & K_{*,*} \end{bmatrix}\right) \tag{3}$$

with $K_{*,f}^{\text{T}} = K_{f,*} = [\kappa(\boldsymbol{x}_1, \boldsymbol{x}_*)\kappa(\boldsymbol{x}_2, \boldsymbol{x}_*) \cdots \kappa(\boldsymbol{x}_N, \boldsymbol{x}_*)]^{\text{T}}$ and $K_{*,*} = \kappa(\boldsymbol{x}_*, \boldsymbol{x}_*)$, the predicted mean and variance of f_* given $\boldsymbol{y}$ are

$$\text{E}[f_* | \boldsymbol{y}] = K_{*,f}(K_{f,f} + \sigma^2 \boldsymbol{I}_N)^{-1} \boldsymbol{y} \tag{4}$$

$$cov[f_* | \boldsymbol{y}] = K_{*,*} - K_{*,f}(K_{f,f} + \sigma^2 \boldsymbol{I}_N)^{-1} K_{f,*} \tag{5}$$

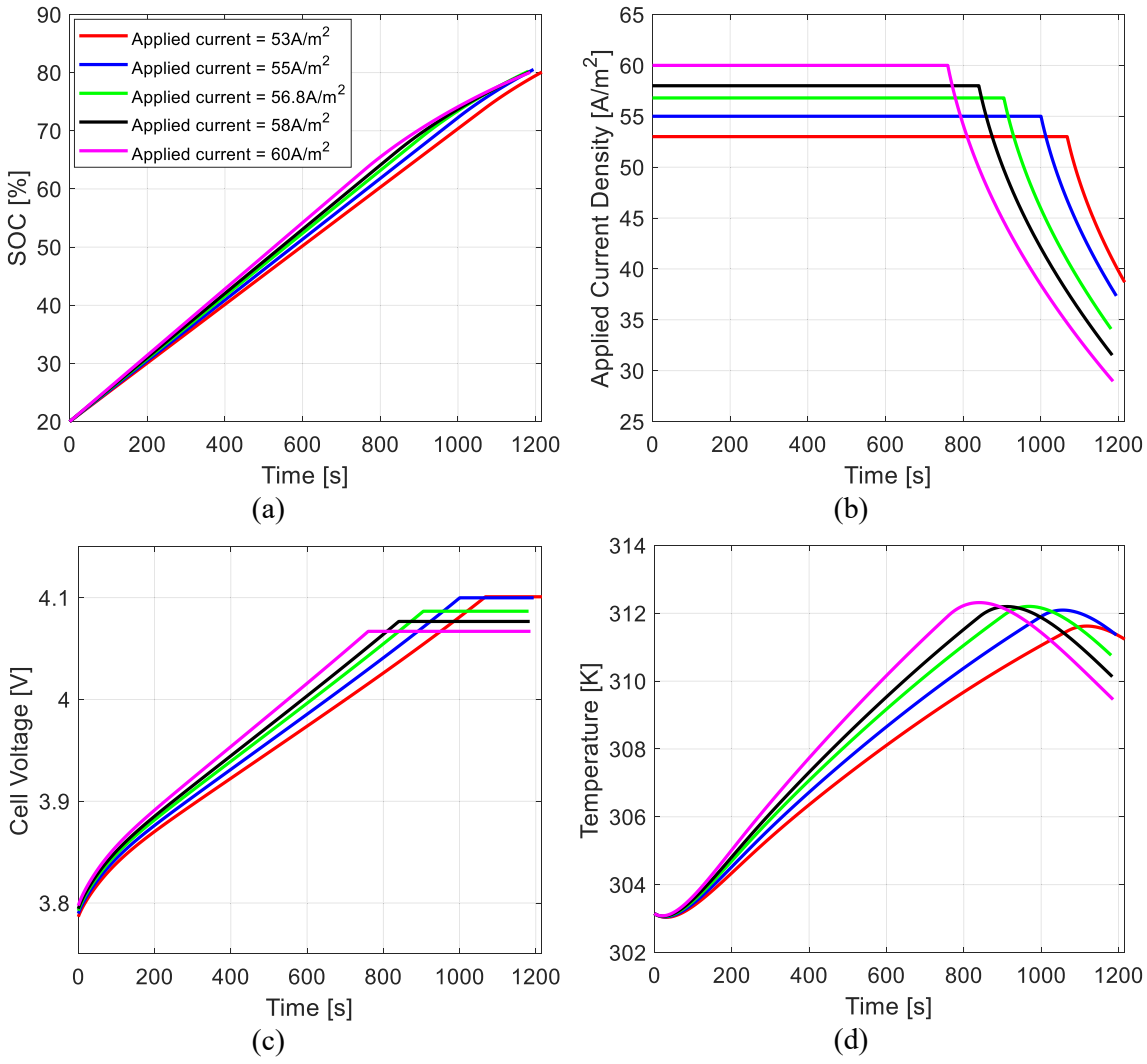

Fig. 2. Charging profiles for one CC-step charging protocols using the applied currents at 53, 55, 56.8, 58, and 60 A/m^2: (a) SOC, (b) applied current density, (c) cell terminal voltage, and (d) cell temperature.

2.2. Acquisition functions

2.2.1. Probability of improvement

The acquisition function of the probability of improvement (PI) is to maximize the probability of improvement over the incumbent $f(\boldsymbol{x}^+)$, where $\boldsymbol{x}^+ = \underset{\boldsymbol{x}_i \in \boldsymbol{X}_{1:t}}{\textit{argminf}}(\boldsymbol{x}_i)$, so that [18,19]

$$\begin{aligned}\alpha_{\mathrm{PI}}(\boldsymbol{x}) &= p(f(\boldsymbol{x}) \leqslant f(\boldsymbol{x}^+) - m) \\ &= \Phi\left(\frac{f(\boldsymbol{x}^+) - u(\boldsymbol{x}) - m}{\sigma(\boldsymbol{x})}\right)\end{aligned} \tag{6}$$

where $\Phi(\cdot)$ is the normal cumulative distribution function; $\mu(\boldsymbol{x})$ and $\sigma(\boldsymbol{x})$ are the posterior predictive marginal GP mean and standard deviation, respectively; and $m \geq 0$ is a margin parameter that selects the evaluation point most likely to provide at least m improvement, which is taken as the estimated noise standard deviation [20].

2.2.2. Expected improvement

The expected improvement (EI) function with respect to the predictive distribution of the Gaussian process enables a balance to the tradeoff of exploitation and exploration. The EI acquisition function is to maximize the improvement which is expressed as [19]

$$\alpha_{\mathrm{EI}}(\boldsymbol{x}) = \begin{cases} (f(\boldsymbol{x}^+) - u(\boldsymbol{x}) - m)\Phi(Z) + \sigma(\boldsymbol{x})\phi(Z) & \text{if } \sigma(\boldsymbol{x}) > 0 \\ 0 & \text{if } \sigma(\boldsymbol{x}) = 0 \end{cases} \tag{7}$$

where

$$Z = \begin{cases} \dfrac{f(\boldsymbol{x}^+) - u(\boldsymbol{x}) - m}{\sigma(\boldsymbol{x})} & \text{if } \sigma(\boldsymbol{x}) > 0 \\ 0 & \text{if } \sigma(\boldsymbol{x}) = 0 \end{cases} \tag{8}$$

$\phi(Z)$ is the normal probability distribution function, and the parameter m is similar as in Eq. (6). The term $(f(\boldsymbol{x}^+) - u(\boldsymbol{x}) - m)\Phi(Z)$ in Eq. (7) is for exploitation and the term $\sigma(\boldsymbol{x})\phi(Z)$ is for exploration.

2.2.3. Lower confidence bound

The Gaussian process lower confidence bound (LCB) acquisition function is defined as [18]

$$\alpha_{\mathrm{LCB}}(\boldsymbol{x}) = \mu(\boldsymbol{x}) - \beta_n^{1/2}\sigma(\boldsymbol{x}) \tag{9}$$

where $\mu(\boldsymbol{x})$ and $\sigma^2(\boldsymbol{x})$ are the posterior predictive marginal GP mean and variance, respectively, and β_n is a hyperparameter for balancing local and global search by favoring regions with low posterior mean and high posterior variance. Although theory indicates that the value of β_n should increase with evaluation number [19,22], in practice its value is commonly selected as a constant between 0.01 and 100 [19]. This article

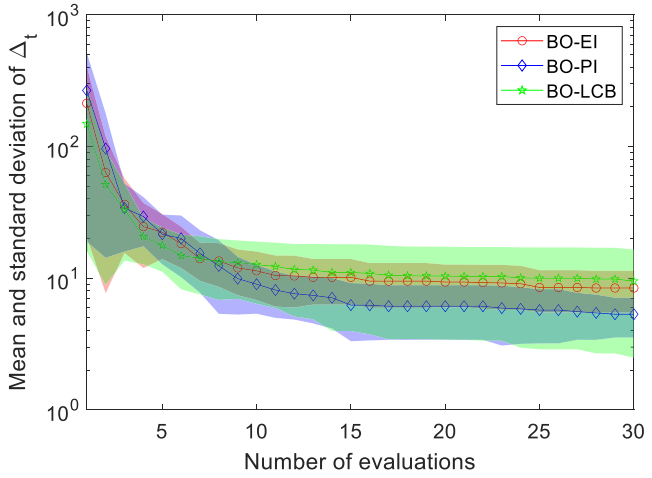

Fig. 3. Mean and standard deviation of the minimum charging time optimized by BO-EI, BO-PI, and BO-LCB as a function of the number of evaluations. Each optimization procedure was repeated 20 times for each acquisition function. The mean minimum charging time t_f obtained by using BO-EI, BO-PI, and BO-LCB after 30 evaluations are comparable, at 1178.5 s (i.e., $\Delta_t = 8.4$), 1175.4 s (i.e., $\Delta_t = 5.3$), and 1179.7 s (i.e., $\Delta_t = 9.6$) respectively, where $\Delta_t = t_f - 1170.1$. The means and standard deviations are plotted separately in Fig. A1.

sets the value $\beta_n = 4$ using the procedure described in the Appendix B.

3. Battery optimal charging problem

This section briefly discusses battery models and the fast-charging optimization problem formulated within the Bayesian optimization framework. A widely used first-principles electrochemical model is considered that describes many of the physicochemical details of battery dynamics, followed by a description of the formulation of the minimum-time charging problem.

3.1. Porous electrode theory-based electrochemical model

The porous electrode theory (PET) model, which is originally developed by Newman and co-workers [34,35], is the most widely used framework for describing physical processes governing lithium-ion battery systems [36]. This article uses LIONSIMBA [32] – a MATLAB implementation of the PET model based on the finite volume method – as a battery simulator for the evaluation of the BO algorithms for the data-driven optimization of battery cycling protocols.

The main governing equations are summarized here, with some equations applying to both cathode and anode. The diffusion of lithium ions within each solid particle is described by [34,35]

$$\frac{\partial}{\partial t}c_s(z,t) = \frac{1}{z^2}\frac{\partial}{\partial z}\left[z^2 D^s_{\text{eff}}\frac{\partial}{\partial z}c_s(z,t)\right] \tag{10}$$

with boundary conditions

$$\frac{\partial}{\partial z}c_s(z,t)\Big|_{z=0} = 0, \frac{\partial}{\partial z}c_s(z,t)\Big|_{z=R_s} = -\frac{j(z,t)}{D^s_{eff}} \tag{11}$$

where t is time, z is the one-dimensional spatial variable; $c_s(z,t)$ is the concentration of the solid particles; R_s is the radius of the solid particles; D^s_{eff} is the effective diffusion coefficients within the particles; and $j(z,t)$ is the ionic flux.

The bulk state of charge (SOC) of the anode is defined as

$$\text{SOC}(t) := \frac{1}{L_n c_s^{max,n}}\int_0^{L_n} c_s(z,t)dz \tag{12}$$

where $c_s^{\max,n}$ is the maximum concentration of lithium ions in the negative electrode.

The flow of lithium ions inside the electrolyte is described by [34,35]

$$\varepsilon\frac{\partial}{\partial t}c_e(z,t) = \frac{\partial}{\partial z}\left[D_{\text{eff}}\frac{\partial c_e(z,t)}{\partial z}\right] + a(1-t_+)j(z,t) \tag{13}$$

where $c_e(z,t)$ is the concentration of lithium ions in the electrolyte, D_{eff} is the effective diffusion coefficient in the electrolyte, a is the ratio of particle surface area to its volume, t_+ is the transference number, and ε is the material porosity.

According to Ohm's law, the conservation of charge in the electrodes can be modeled as

$$\frac{\partial}{\partial z}\left[\sigma_{\text{eff}}\frac{\partial}{\partial z}\Phi_s(z,t)\right] = aFj(z,t) \tag{14}$$

where $\Phi_s(z,t)$ is the solid potential, F is Faraday's constant, and σ_{eff} is the effective conductivity of the electrodes. The voltage of the Li-ion cell can be calculated from

$$V(t) = \Phi_s(0,t) - \Phi_s(L,t) \tag{15}$$

where $z = 0$ and $z = L$ correspond to the current collector at the cathode and anode sides.

The temperature dynamics are described by

$$\rho C_p\frac{\partial}{\partial t}T(z,t) = \frac{\partial}{\partial z}\left[\lambda\frac{\partial}{\partial z}T(z,t)\right] + Q_{\text{ohm}}(z,t) + Q_{\text{rxn}}(z,t) + Q_{\text{rev}}(z,t) \tag{16}$$

where λ is the thermal conductivity, C_p is the specific heat, ρ is the material density, and the terms $Q_{\text{ohm}}(z,t)$, $Q_{\text{rev}}(z,t)$, and $Q_{\text{rxn}}(z,t)$ represent ohmic, reversible, and reaction heat sources [32,35].

The above equations are coupled through ionic flux, which is described via the Butler–Volmer equation

$$j_{int}(z,t) = 2\frac{i_{0,int}}{F}sinh\left[\frac{0.5F}{RT(z,t)}\eta_{int}\right] \tag{17}$$

where η_{int} is the electrode overpotential and $i_{0,\text{int}}$ is the exchange current density given by

$$i_{0,int} = Fk_{\text{eff}}\sqrt{c_e(z,t)\left(c_s^{max} - c_s^*(z,t)\right)c_s^*(z,t)} \tag{18}$$

where k_{eff} is the effective kinetic reaction rate, and $c_s^*(z,t)$ is the surface concentration of the solid particles.

The constraints on current, voltage, and temperature are implemented in a manner that does not increase the number of degrees of freedom in the cycling protocol optimization. The constraint on the current is handled directly, by only allowing the BO to choose values within the current constraints. During charging, the satisfaction of the voltage and temperature constraints is continuously monitored in real time. If the voltage or temperature reaches its maximum allowed value, then the current is reduced only as much as needed to satisfy both the voltage and temperature constraints. This way of embedding constraints into the battery operation does not increase the number of degrees of freedom of the optimization variables, which enables BO to have faster convergence to produce results of higher accuracy for the same number of evaluations, or for the same degree of optimality to be achieved with fewer evaluations.

3.2. Minimum time charging problem

The objective is to solve the battery charging problem in minimum time given a battery model and operating constraints. Specifically, the minimum charging time problem is formulated as

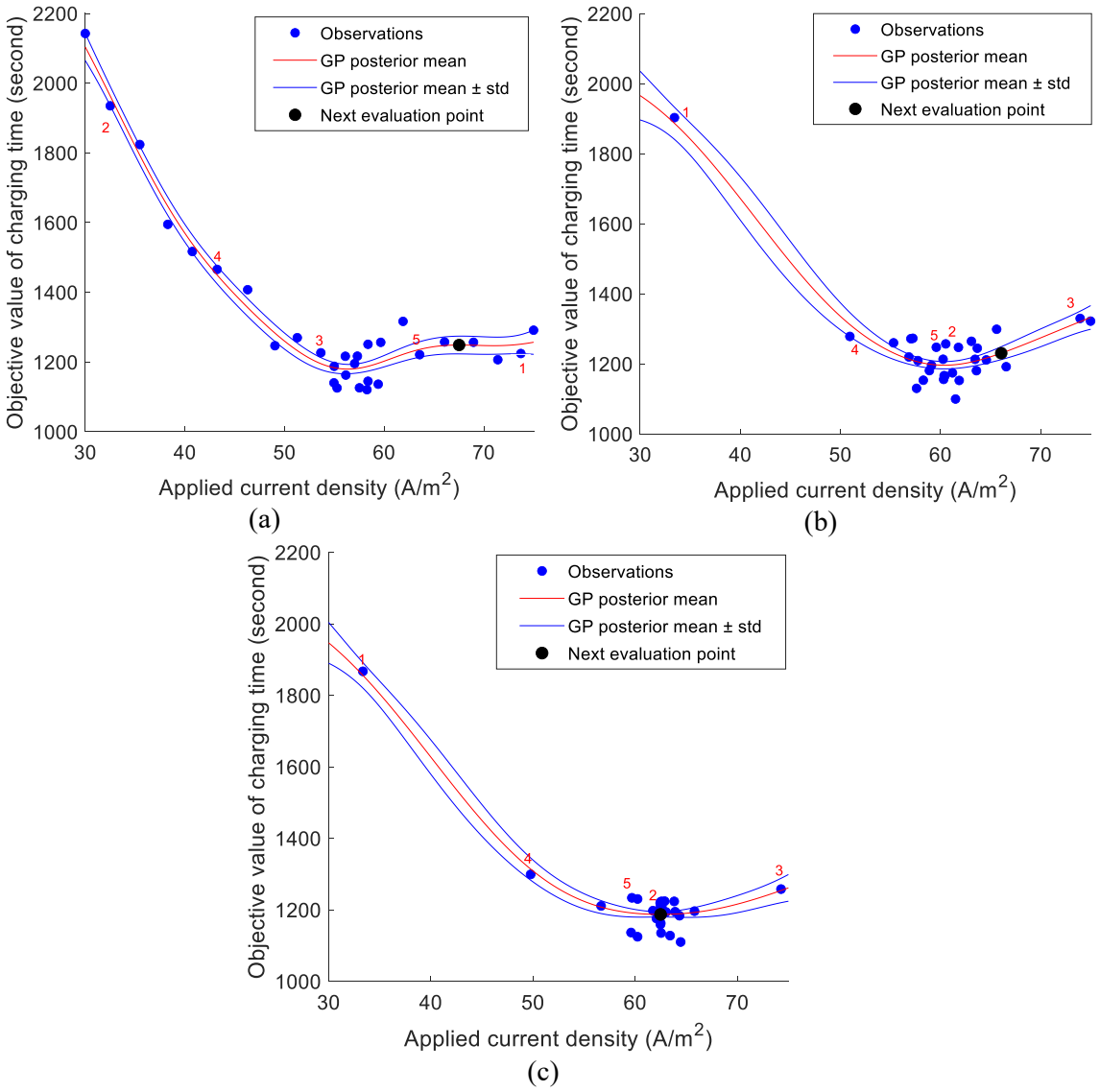

Fig. 4. Comparison of (a) EI, (b) PI, and (c) LCB acquisition functions for the minimum time charging protocol optimization of a CC-CV charging profile.

$$\min_{I(t)} \{t_f\} \tag{19}$$

$$\text{such that} \begin{cases} \text{battery dynamics in (10) - (17)} \\ T_{\text{cell}}(t_0) = T_0 \\ \text{SOC}(t_f) = \text{SOC}_{\text{ref}} \\ V(t) \leqslant V^{max},\ T_{\text{cell}}(t) \leqslant T_{\text{cell}}^{\max} \\ I(t) \in [I_{min}, I_{max}] \end{cases} \tag{20}$$

where $t_0 = 0$ and t_f are the initial and final times of the charging process, T_0 is the initial value for the temperature, SOC_{ref} is the reference of SOC at which the charging is considered completed, $[I_{min}, I_{max}]$ is the bound interval for the charging current, and $V^{\max}$ and $T_{\text{cell}}^{\max}$ are upper bounds for the voltage and temperature.

Multi-constant-current-step charging protocols are considered here, in which $I(t)$ is a series of constant current steps which, for a fixed number of steps, are parameterized by the values of the current within each step and the times for switching between each step. This structure can be written as $I_1(t_1)$-…-$I_i(t_i)$-$I_{i+1}(t_f)$, where I_i, $i = 0, 1, 2, \ldots$, is the ith applied current density, t_i is the charging time at which the current switches, and t_f is the final charging time. If the cell voltage during charging reaches its maximum allowed value, or the cell temperature during charging reaches 99.5% of its maximum value,[3] the charging switches from constant current to constant voltage (see the last paragraph of Section 3.1). This approach embeds the inequality constraints on the voltage and temperature in Eq. (20) into the battery's operation. The battery operation always starts at the same temperature and always operates until the SOC reaches SOC_{ref}, which also sets the finite time t_f. This approach reduces the explicit constraints in Eq. (20) to only being the minimum and maximum values of the current in each time step, greatly simplifying the formulation and implementation of the Bayesian optimization.

4. Results and discussion

This section explores ways to increase rate of convergence to an optimal charging protocol or, equivalently, to minimize the number of battery cycling experiments needed to reach the optimal charging protocol within a specified degree of accuracy. Our goal is to obtain a

[3] This strategy is known as a "soft limit" or "soft constraint" in the optimal control literature, and is widely used to simplify calculations [37]. The 99.5% is a design parameter set just low enough that the maximum allowable temperature is not reached during operation.

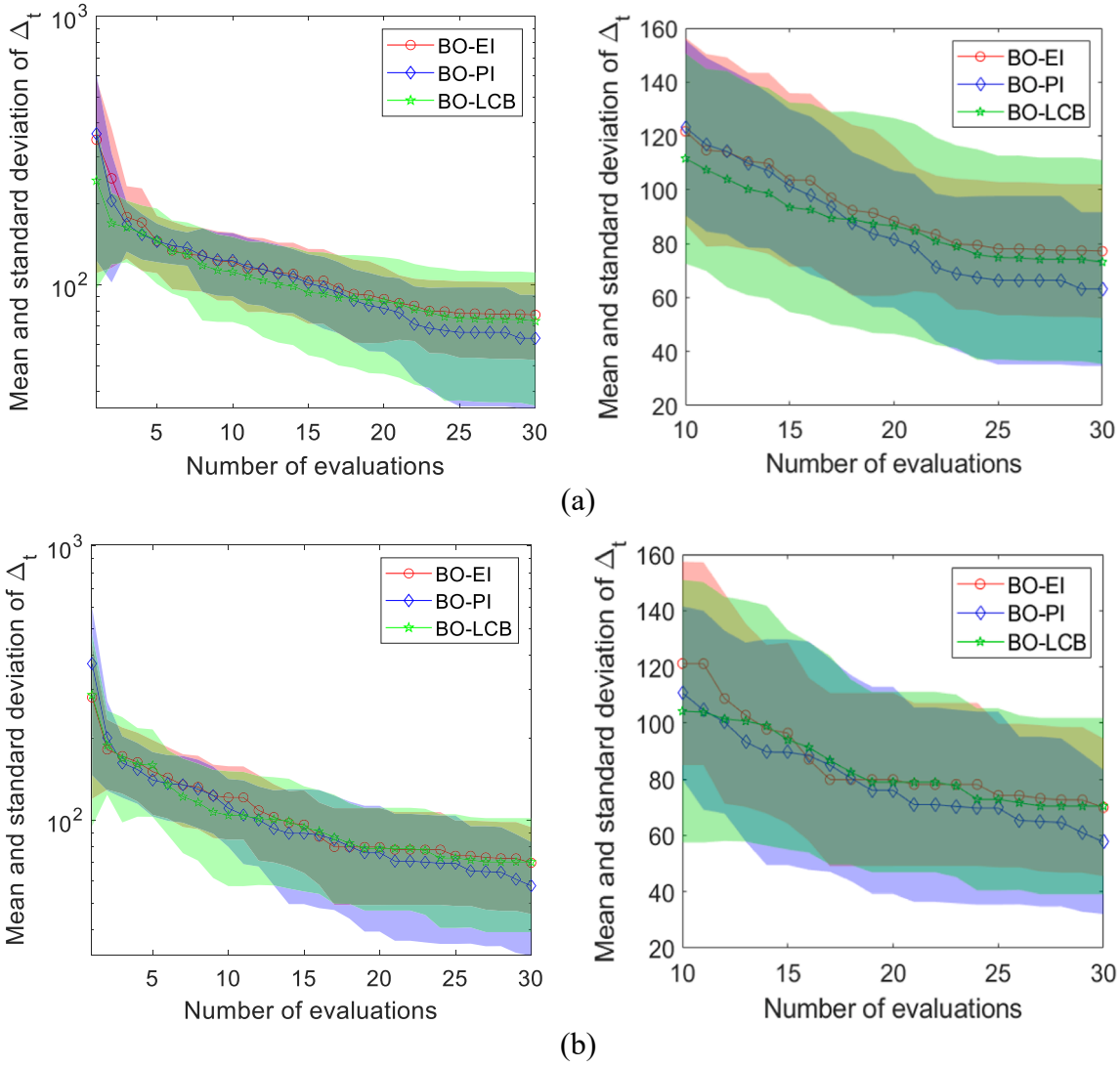

Fig. 5. The mean and standard deviation of the MCT obtained by BO-EI, BO-PI, and BO-LCB as a function of the number of evaluations for multi-constant-current-step charging protocols for (a) two CC steps, for which the optimal charging protocol $I_1(t_1) - I_2 = 75.0$ A/m^2 (400.1 s)-51.8 A/m^2 and the corresponding MCT is 1057.5 s where $\Delta_t = t_f - 1057.5$, and (b) three CC steps, for which the optimal charging protocol $I_1(t_1) - I_2(t_2) - I_3 = 74.7$ A/m^2 (397.1 s)-52.4 A/m^2(745.9 s)-73.4 A/m^2 and the corresponding MCT is 1043.5 s where $\Delta_t = t_f - 1043.5$. Each procedure was repeated 20 times for each acquisition function. The plots at the right are zoom-ins of the plots on the left, to provide more resolution for larger numbers of evaluations. The means and standard deviations are plotted separately in Fig. A2. The mean MCT t_f produced by BO-EI, BO-PI, and BO-LCB are 1134.8, 1118.7, and 1130.7 s respectively for the two-step charging protocols, and 1116.7, 1107.2, and 1117.0 s respectively for the three-step protocols.

Table 1
Best and mean of minimum charging times produced by the BO approach for the one, two, and three CC-step protocols.

	One CC-step protocol	Two CC-step protocol	Three CC-step protocol
Best minimum charging time	1170.1 s	1057.5 s	1043.5 s
Mean minimum charging time	1175.4 s	1118.7 s	1107.2 s

minimum time charging protocol that charges the battery from 20% state of charge (SOC) to 80% SOC, while keeping the cell temperature and cell terminal voltage within operational constraints. The noise-to-signal ratio σ in Eq. (1) is 5% in this work. The initial cell temperature is 303.15 K and the ambient temperature is 300 K. The values of the constraint parameters are $V^{\max} = 4.1$V , $T_{\text{cell}}^{\max} = 313.15$K , and $[I_{\min}, I_{\max}] = [30, 75]$A/m^2 .

We examine the performance of various acquisition functions (i.e., EI, PI, and LCB) for the minimum time charging problem using the electrochemical model in Section 3, for a graphite anode/$LiCoO_2$ (LCO) cathode cell, with the parameter values given in [32]. LIONSIMBA [32], which is a MATLAB implementation of the PET model based on the finite volume method, is used in place of experiments for evaluation of the data-driven methods for the optimization of battery cycling protocols.

4.1. Case study 1: Single-constant-current-step (aka CC-CV) charging protocol

The objective in this subsection is (i) to validate the performance of Bayesian optimization on the minimum time charging problem, and (ii) to compare the performance of using the acquisition functions of EI, PI, and LCB for exploiting and exploring the parameter space of charging protocols. The CC-CV charging protocol is first considered, followed by the multi-constant- current step protocols.

Before presenting the BO results, it is instructive to first discuss the simulation results for noise-free CC-CV simulations. Figs. 1 and 2 plot the SOC, applied current density, voltage, and temperature profiles for initial applied currents of {30, 40, 50, 60, 75} A/m^2 and {53, 55, 56.8,

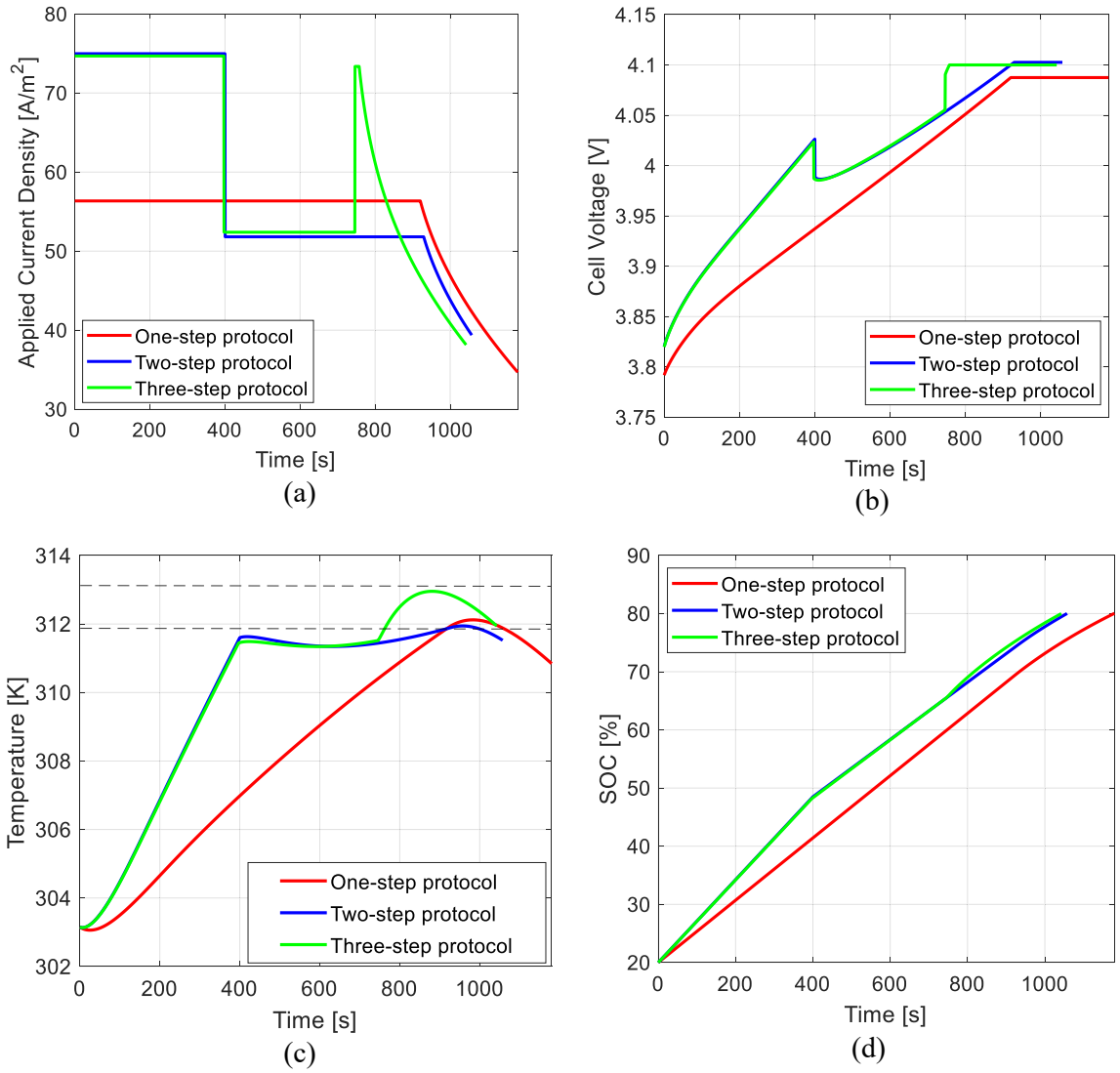

Fig. 6. The best charging protocols provided by BO-PI for one, two, and three CC steps after 30 evaluations: (a) applied current density, (b) cell terminal voltage, (c) cell temperature, and (d) SOC. The dashed lines in the cell temperature are the hard limit of temperature (i.e., upper bound of temperature $T_{\text{cell}}^{\max}$) and soft limit of the temperature (i.e., 99.5% of upper bound of temperature $T_{\text{cell}}^{\max}$) that triggers the charging switching from CC to CV step. The MCT for the one, two, and three CC-step protocols is 1170.1 s, 1057.5 s, and 1043.5 s.

58, 60} A/m^2 respectively for the deterministic battery (i.e., noise-free observations). When the initial applied currents are between 30 and 40 A/m^2, the CC charging is used throughout the whole process, without hitting the voltage or temperature limits. When the initial applied currents are between 40 and 55 A/m^2, the charging process first hits the voltage limit, which triggers the charging switching from CC to CV; when the initial applied currents are between 55 and 75 A/m^2, the charging process first hits the soft limit on the temperature (i.e., 99.5% of upper bound of temperature $T_{\text{cell}}^{\max}$), triggering the charging to switch from CC to CV. As shown in Figs. 1 and 2, the optimal charging current is 56.8 A/m^2, and the corresponding minimum charging time is 1170.1 s.

Given the budget of 30 evaluations, the mean and standard deviation of minimum charging time (MCT) for the minimum-time charging protocols optimized by using the EI, PI, and LCB acquisition functions are plotted as a function of the number of evaluations in Fig. 3. As the number of evaluations increases, the mean MCT monotonically decreases for all three acquisition functions. The MCT drops the most during the first 7 evaluations, with relatively modest further reductions during additional evaluations. For the same number of evaluations within the range from 8 to 30, the BO-PI had faster charging time than BO-EI and BO-LCB. Also, for the same number of evaluations within the range from 9 to 30, the performance of BO-PI and BO-EI is more consistent than BO-LCB, while providing lower mean minimum charging time.

Fig. 4 visualizes the sampling behavior to reach the optimal charging profile, along with the corresponding GP modeling for the objective function, by the utilization of acquisition functions of EI, PI, and LCB, respectively. The EI, PI, and LCB acquisition functions provide distinct sampling behaviors over time. The exploratory behavior of PI and LCB acquisition functions did not sample the region around the applied current density from 35 A/m^2 to 48 A/m^2 once PI and LCB determined there was a minimum chance of improvement (Fig. 4bc), whereas the EI acquisition function continued to explore (Fig. 4a). The LCB acquisition function became trapped near 62 A/m^2 after several iterations (Fig. 4c), which occurred because its exploitation term $\mu(\boldsymbol{x})$ in Eq. (9) is more dominant than the exploration item and $\sigma^2(\boldsymbol{x})$, which results in the sampling behavior, tended to concentrate around the optimum of the past sampled points.

For noisy observations, to avoid maximizing the probability or expected improvement over an unreliable sample, the BO methods probabilistically repeat samples to obtain more reliable estimates. This resampling is observed in the sampling behaviors of all three acquisition

functions. Resampling is performed in the promising area around the applied current densities of 56 A/m^2, 60 A/m^2, and 62 A/m^2 by the acquisition functions of EI, PI, and LCB respectively, as shown in Fig. 4.

4.2. Case study 2: Multi-constant-current-step charging protocol

The multi-constant-current-step protocols $I_1(t_1)-\ldots-I_i(t_i)-I_{i+1}(t_f)$, $i = 1, 2$, are considered in this subsection given a budget of 30 evaluations. I_1, t_1, I_2 are the variables to be optimized by the BO in the case of a two CC-step charging protocol and I_1, t_1, I_2, t_2, I_3 for the case of a three CC-step protocol. For the same number of evaluations from 19 to 30, BO-PI had faster charging time than BO-LCB and BO-EI for both the two- and three-step charging protocols. The MCT decreases with increasing number of current steps (Table 1), as more degrees of freedom become available for optimization.

The best MCT was achieved by the PI acquisition function for one, two, and three CC-step protocols, with the applied current density, state of charge, cell voltage, and cell temperature plotted in Fig. 6. The charging processes for one and three CC-step protocols first hit the soft limit of the temperature (i.e., 99.5% of the upper bound of the temperature $T_{\text{cell}}^{\max}$), which enables the charging to switch from CC to CV, while the two CC-step charging first hits the voltage limit that triggered its charging to switch from CC to CV. In both cases, the maximum charging current is applied until the switching point (hitting the voltage or temperature limits). Compared with the MCTs optimized for one and two CC-step charging protocols, the three CC-step protocol charged 126.6 s and 14.0 s faster, respectively. The mean and best MCT are farther apart for the three than the two CC-step protocols (Table 1), and for the two than the one CC-step protocols. The difference between the mean and best MCT for three CC-step protocols is 63.7 s, which are 58.4 and 2.5 s larger than that of one CC-step (5.3 s) and two CC-step protocols (61.2 s), respectively. The reason for the differences is that, for a fixed number of evaluations, the higher dimension of the parameter spaces, the larger the variance of results produced by the BO methods. In addition, the increase in the difference between the mean and the best charging time – a measure of the uncertainty – is modest when increasing the number of degrees of freedom in the optimization when going from two- to three-CC-step protocols.

For one CC-step charging protocols, the Bayesian optimization reduced the charging time from $t_f = \sim$2000 s to $t_f = 1170.1$ s (Fig. 4 and Table 1), which is a reduction in charging time of $\sim$ 41%. For two CC-step and three CC-step protocols, the charging time was reduced from $\sim$ 2000 s to 1057.5 s and 1043.5 s (Table 1), respectively, which are reductions of $\sim$ 47% and $\sim$ 48%. Increasing the number of CC-steps from one to two resulted in a significant reduction in charging time, whereas including a third CC-step led to marginal improvement. The three CC-step protocol has more variations in applied current and temperature than the two CC-step protocol (Fig. 6), suggesting that the two-step protocol may have less degradation in practice. Given that the reduction in the charging time from increasing the number of CC-steps from two to three is marginal, a reasonable approach would be to use the two CC-step protocol.

For practical applications, the proposed BO-based approaches just need an initial set of data for training the machine learning model. Specifically, a surrogate model of Gaussian process (GP) is trained on the initial dataset; and an acquisition function is constructed using the information of the learned GP model to probe the next data sample. The data sample is then incorporated into the dataset to update the GP model. These procedures are repeated until obtaining optimal charging protocols or reaching the maximum iteration step.

5. Conclusions

In this article, a Bayesian optimization strategy is examined for the minimum time battery charging problem in the presence of voltage and temperature constraints. We explore three types of acquisition functions (i.e., expected improvement, probability of improvement, and lower confidence bound) for minimizing the charging time for single- and multi-constant-current-step charging profiles. The BO strategy was evaluated for a porous electrode theory-based electrochemical model. The BO-based charging approaches are sample-efficient and do not require first-principles models. The probability-of-improvement acquisition function has lower mean and best minimum changing time than the expected-improvement and lower-confidence-bound acquisition functions. We quantified the decrease in the minimum charging time with increasing number of current steps – the three CC-step protocol charged 126.6 s and 14.0 s faster than the one and two CC-step protocols, respectively. We also quantified the increase in the uncertainty in the minimum charging time with increasing number of degrees of freedom in the optimization. For the best-performing acquisition function, the difference between the mean and best MCT for the three-CC-step protocol is 63.7 s, which are 58.4 s and 2.5 s larger than that of one CC-step (5.3 s) and two-CC-step protocols (61.2 s), respectively. The increase in the difference between the mean and the best charging time – a measure of the uncertainty – is modest when increasing the number of degrees of freedom in the optimization when going from two- to three-CC-step protocols.

In terms of future work, the BO strategy can be used to optimize smooth fast charging protocols by parameterizing the time-varying current in terms of a basis function expansion or a spline [e.g., [8-11]]. The BO strategy can also be applied to include the optimization of battery design parameters, which is relevant for next-generation electrode and electrolyte chemistries (e.g., Si anodes, S cathodes, and solid-state electrolytes) with unfamiliar electrochemical behaviors near commercial deployment [38,39].

CRediT authorship contribution statement

Benben Jiang: Conceptualization, Methodology, Software, Validation, Formal analysis, Data curation, Writing – original draft, Visualization. **Marc D. Berliner:** Methodology, Software, Data curation, Writing – original draft. **Kun Lai:** Validation, Formal analysis, Data curation, Visualization. **Patrick A. Asinger:** Software, Writing – original draft. **Hongbo Zhao:** Writing – original draft. **Patrick K. Herring:** Writing – original draft. **Martin Z. Bazant:** Funding acquisition, Writing – original draft. **Richard D. Braatz:** Conceptualization, Supervision, Project administration, Funding acquisition, Writing – original draft.

Declaration of Competing Interest

The authors declare that they have no known competing financial interests or personal relationships that could have appeared to influence the work reported in this paper.

Acknowledgements

Financial support from the Toyota Research Institute is acknowledged.

Appendix A

Figs. A1 and A2 are alternative ways to plot the data in Figs. 3 and 5.

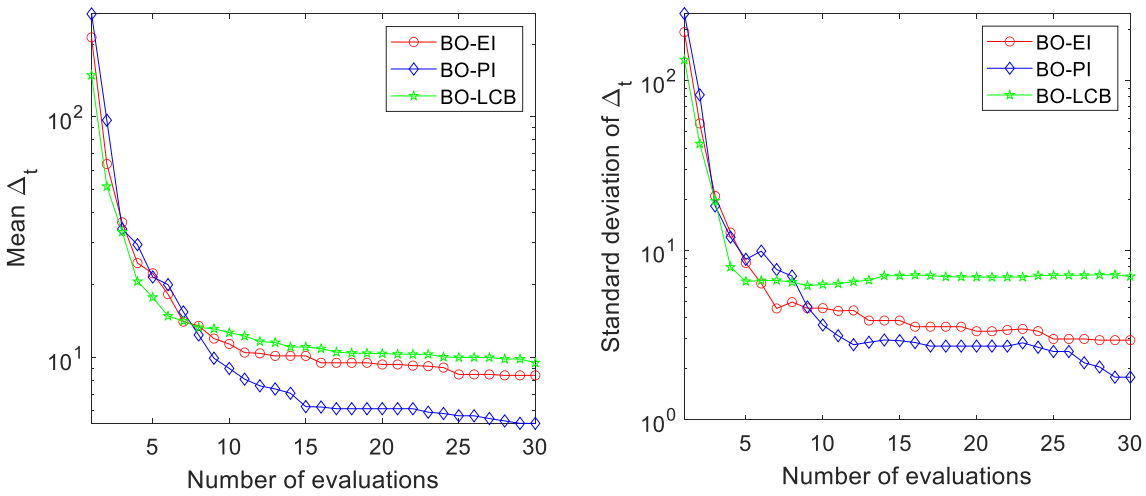

Fig. A1. Mean (left) and standard deviation (right) of the minimum charging time for one CC-step in the CC-CV protocol optimized by BO-EI, BO-PI, and BO-LCB as a function of the number of evaluations. Each optimization procedure was repeated 20 times for each acquisition function. The mean minimum charging time t_f obtained by using the BO-EI, BO-PI, and BO-LCB methods after 30 evaluations are comparable, at 1178.5 s (i.e., $\Delta_t = 8.4$), 1175.4 s (i.e., $\Delta_t = 5.3$), and 1179.7 s (i.e., $\Delta_t = 9.6$) respectively, where $\Delta_t = t_f - 1170.1$.

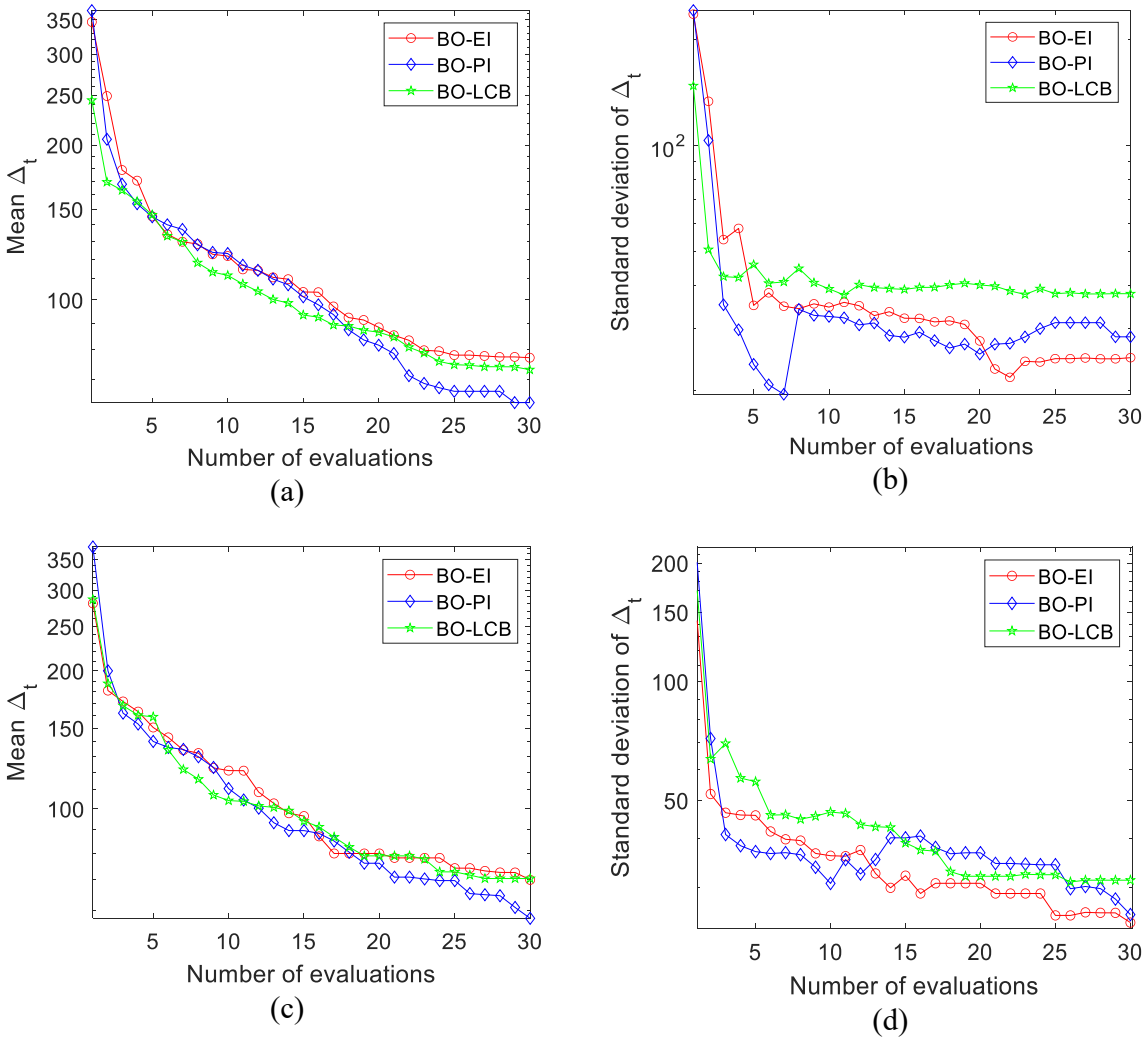

Fig. A2. The performance of minimum charging time optimized by BO-EI, BO-PI, and BO-LCB as a function of evaluation number for multi-constant-current-step charging protocol: (a) mean and (b) standard deviation of the MCT for two CC-step charging, in which the optimal charging protocol $I_1(t_1) - I_2 = 75.0$ A/m^2 (400.1 s)-51.8 A/m^2 and the corresponding MCT is 1057.5 s, and (c) mean and (d) standard deviation of the MCT for three CC-step charging, in which the optimal charging protocol $I_1(t_1) - I_2(t_2) - I_3 = 74.7$ A/m^2 (397.1 s)-52.4 A/m^2(745.9 s)-73.4 A/m^2 and the corresponding MCT is 1043.5 s. The same procedure was repeated 20 times for each acquisition function.

Appendix B

Fig. B1 depicts the performance of BO-LCB as a function of β_n , a hyperparameter in the LCB acquisition function for balancing the exploration and exploitation (see Eq. (9)), for the minimizing the charging time. It can be observed that $\beta_n = 4$ is an appropriate value for BO-LCB for the fast-charging optimization.

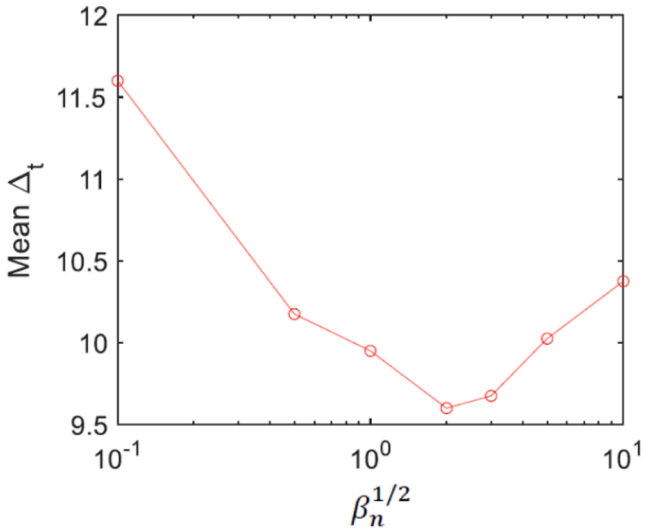

Fig. B1. The mean minimum charging time obtained by the BO-LCB approach as a function of $\beta_n^{1/2} = 0.1$, 0.5, 1, 2, 3, 5, and 10 after 30 evaluations, for the MCT optimization. Each optimization procedure was repeated 20 times for each value of β_n .

References

[1] Waag W, Fleischer C, Sauer DU. Critical review of the methods for monitoring of lithium-ion batteries in electric and hybrid vehicles. J Power Sources 2014;258:321–39.

[2] Cano ZP, Banham D, Ye S, Hintennach A, Lu J, Fowler M, et al. Batteries and fuel cells for emerging electric vehicle markets. Nat Energy 2018;3(4):279–89.

[3] Lam F, Allam A, Joe WT, Choi Y, Onori S. Offline multi-objective optimization for fast charging and reduced degradation in lithium-ion battery cells using electrochemical dynamics. IEEE Control Syst Lett 2021;5(6):2066–71.

[4] Yang X-G, Wang C-Y. Understanding the trilemma of fast charging, energy density and cycle life of lithium-ion batteries. J Power Sources 2018;402:489–98.

[5] Feng X, Ouyang M, Liu X, Lu L, Xia Y, He X. Thermal runaway mechanism of lithium ion battery for electric vehicles: A review. Energy Storage Mater 2018;10:246–67.

[6] Attia PM, Grover A, Jin N, Severson KA, Markov TM, Liao Y-H, et al. Closed-loop optimization of fast-charging protocols for batteries with machine learning. Nature 2020;578(7795):397–402.

[7] Chu Z, Feng X, Lu L, Li J, Han X, Ouyang M. Non-destructive fast charging algorithm of lithium-ion batteries based on the control-oriented electrochemical model. Appl Energy 2017;204:1240–50.

[8] Suthar B, Northrop PW, Braatz RD, Subramanian VR. Optimal charging profiles with minimal intercalation-induced stresses for lithium-ion batteries using reformulated pseudo-two-dimensional models. J Electrochem Soc 2014;161:F3144–55.

[9] Yin Y, Choe S-Y. Actively temperature controlled health-aware fast charging method for lithium-ion battery using nonlinear model predictive control. Appl Energy 2020;271:115232.

[10] Zhang C, Jiang J, Gao Y, Zhang W, Liu Q, Hu X. Charging optimization in lithium-ion batteries based on temperature rise and charge time. Appl Energy 2017;194:569–77.

[11] Yin Y, Bi Y, Hu Y, Choe S-Y. Optimal fast charging method for a large-format lithium-ion battery based on nonlinear model predictive control and reduced order electrochemical model. J Electrochem Soc 2020;167(16):160559.

[12] Xu M, Wang R, Zhao P, Wang X. Fast charging optimization for lithium-ion batteries based on dynamic programming algorithm and electrochemical-thermal-capacity fade coupled model. J Power Sources 2019;438:227015.

[13] Li Y, Vilathgamuwa M, Wikner E, Wei Z, Zhang X, Thiringer T, et al. Electrochemical model-based fast charging: Physical constraint-triggered PI control. IEEE Trans Energy Convers 2021, doi: 10.1109/TEC.2021.3065983.

[14] Romagnoli R, Couto LD, Goldar A, Kinnaert M, Garone E. A feedback charge strategy for Li-ion battery cells based on reference governor. J Process Control 2019;83:164–76.

[15] Perez HE, Dey S, Hu X, Moura SJ. Optimal charging of Li-ion batteries via a single particle model with electrolyte and thermal dynamics. J Electrochem Soc 2017;164(7):A1679–87.

[16] Smith RB, Bazant MZ. Multiphase porous electrode theory. J Electrochem Soc 2017;164(11):E3291–310.

[17] Park, S., Pozzi, A., Whitmeyer, M., Perez, H., Joe, W.T., Raimondo, D.M. and Moura, S. Reinforcement learning-based fast charging control strategy for Li-ion batteries. *IEEE Conference on Control Technology and Applications*, 100–107, 2020.

[18] Shahriari B, Swersky K, Wang Z, Adams RP, de Freitas N. Taking the human out of the loop: A review of Bayesian optimization. Proc IEEE 2016;104:148–75.

[19] Archetti F, Candelieri A. Bayesian Optimization and Data Science. New York, U.S.: Springer International Publishing; 2019.

[20] Liu J, Jiang C, Zheng J. Batch Bayesian optimization via adaptive local search. Applied Intelligence 2021;51(3):1280–95.

[21] Martinez-Cantin R, de Freitas N, Brochu E, Castellanos J, Doucet A. A Bayesian exploration-exploitation approach for optimal online sensing and planning with a visually guided mobile robot. Autonomous Robots 2009;27(2):93–103.

[22] Brochu, E., Cora, V.M. and De Freitas, N. A tutorial on Bayesian optimization of expensive cost functions, with application to active user modeling and hierarchical reinforcement learning. arXiv preprint arXiv:1012.2599, 2010.

[23] Garnett R, Osborne MA, Roberts SJ. Bayesian optimization for sensor set selection. In: Proceedings of the 9th ACM/IEEE International Conference on Information Processing in Sensor Networks; 2010. p. 209–19.

[24] Snoek, J., Larochelle, H. and Adams, R. P. Practical Bayesian optimization of machine learning algorithms. *Proceedings of Neural Information Processing Systems*, 2960–2968, 2012.

[25] Leng F, Tan CM, Pecht M. Effect of temperature on the aging rate of Li ion battery operating above room temperature. Sci Rep 2015;5(1):1–12.

[26] Klein R, Chaturvedi NA, Christensen J, Ahmed J, Findeisen R, Kojic A. Optimal charging strategies in lithium-ion battery. In: Proceedings of the American Control Conference; 2011. 382–87.

[27] Finegan DP, Quinn A, Wragg DS, Colclasure AM, Lu X, Tan C, et al. Spatial dynamics of lithiation and lithium plating during high-rate operation of graphite electrodes. Energy Environ Sci 2020;13(8):2570–84.

[28] Gao T, Han Yu, Fraggedakis D, Das S, Zhou T, Yeh C-N, et al. Interplay of lithium intercalation and plating on a single graphite particle. Joule 2021;5(2):393–414.

[29] Li Y, Feng X, Ren D, Ouyang M, Lu L, Han X. Thermal runaway triggered by plated lithium on the anode after fast charging. ACS Appl Mater Interfaces 2019;11(50):46839–50.
[30] Harris SJ, Timmons A, Baker DR, Monroe C. Direct in situ measurements of Li transport in Li-ion battery negative electrodes. Chem Phys Lett 2010;485(4-6):265–74.
[31] Thomas-Alyea KE, Jung C, Smith RB, Bazant MZ. In situ observation and mathematical modeling of lithium distribution within graphite. J Electrochem Soc 2017;164(11):E3063–72.
[32] Torchio M, Magni L, Gopaluni RB, Braatz RD, Raimondo DM. LIONSIMBA: A Matlab framework based on a finite volume model suitable for Li-ion battery design, simulation, and control. J Electrochem Soc 2016;163:A1192–205.
[33] Rasmussen CE, Christopher KIW. Gaussian Processes for Machine Learning. Cambridge, U.S.: The MIT Press; 2005.
[34] Newman J, Tiedemann W. Porous-electrode theory with battery applications. AIChE J 1975;21(1):25–41.
[35] Fuller TF, Doyle M, Newman J. Simulation and optimization of the dual lithium-ion insertion cell. J Electrochem Soc 1994;141(1):1–10.
[36] Fuller TF, Doyle M, Newman J. Relaxation phenomena in lithium-ion-insertion cells. J Electrochem Soc 1994;141(4):982–90.
[37] Richards A. Fast model predictive control with soft constraints. Eur J Control 2015;25:51–9.
[38] Zhu K, Wang C, Chi Z, Ke F, Yang Y, Wang A, et al. How far away are lithium-sulfur batteries from commercialization? Front Energy Res 2019;7. https://doi.org/10.3389/fenrg.2019.00123.
[39] Gent WE, Abate II, Yang W, Nazar LF, Chueh WC. Design rules for high-valent redox in intercalation electrodes. Joule 2020;4(7):1369–97.